World Academy of Science, Engineering and Technology
International Journal of Mechanical and Mechatronics Engineering
Vol:13, No:12, 2019

Effect of Viscous Dissipation and Axial Conduction in Thermally Developing Region of the Channel Partially Filled with a Porous Material Subjected to Constant Wall Heat Flux

D Bhargavi, J. Sharath Kumar Reddy

Abstract**—**The present investigation has been undertaken to assess the effect of viscous dissipation and axial conduction on forced convection heat transfer in the entrance region of a parallel plate channel with the porous insert attached to both walls of the channel. The flow field is unidirectional. Flow in the porous region corresponds to Darcy-Brinkman model and the clear fluid region to that of plane Poiseuille flow. The effects of the parameters Darcy number, *Da*, Peclet number, *Pe*, Brinkman number, *Br* and a porous fraction γ_p on the local heat transfer coefficient are analyzed graphically. Effects of viscous dissipation employing the Darcy model and the clear fluid compatible model have been studied.

Keywords**—**Porous material, channel partially filled with a porous material, axial conduction, viscous dissipation.

I. Introduction

STUDIES involving the flow of fluid and heat transfer through porous media find applications in diverse situations like electronic components cooling and assessment of risk factors in nuclear waste disposal.

A system that consists of both a fluid saturated porous material and fluid is called composite system. The problems of fluid and heat flow in these systems constitute a significant type of problem which is related to porous matrix convection. The interaction of the flow and temperature fields in the open and porous phases affects the phenomena of convection in the composite systems. Since completely filling the system with the porous medium is not desirable in problems of convective heat transfer in the porous medium, systems that are partially filled are the better alternatives to get enhanced heat transfer. This class of problems finds applications in situations of thermal engineering such as geothermal systems with fault zones, the stored grains cooling and removal of heat in nuclear debris beds.

Several studies [1]-[4] have shown that axial conduction term becomes significant in the equation of energy at low Peclet number in the case of forced convection in the ducts. Further, the thermal field significantly gets altered because of axial conduction. Several researchers [5]-[9] studied the problem of forced convection considering axial conduction effect, under different conditions. In particular, [10] studied the problem of heat transfer in the entrance region for a viscous incompressible fluid in both two dimensional channel and a circular cylindrical tube taking into consideration axial conduction term. Nguyen [11] studied the same problem with boundary conditions of uniform temperature and uniform heat flux at the walls. Ramjee and Satyamurty [3] studied local and average heat transfer in the thermally developing region of an asymmetrically heated channel.

Hooman et al. [12] studied thermally developing Brinkman-Brinkman forced convection in rectangular ducts with isothermal walls. Kuznetsov et al. [13] studied thermally developing forced convection in a circular duct filled with porous material with axial conduction and viscous dissipation effects. They [13] used constant wall temperature boundary conditions at the walls. Nield et al. [14] investigated the effects of viscous dissipation, axial conduction with uniform temperature at the walls, on thermally developing forced convection heat transfer in a parallel plate channel fully filled with a porous medium.

In view of the above, this paper studied forced convection in a channel partially filled with a porous medium with the effect of axial conduction and viscous dissipation subjected to constant wall heat flux. Flow field is assumed to be fully developed and the entrance effects are considered in the thermal field. Numerical solutions for the two dimensional energy equations in both the fluid and porous regions have been obtained using the successive accelerated replacement (SAR) numerical scheme [3], [15], [16]. The effects of important parameters on temperature and local Nusselt number have been studied.

II. Mathematical Formulation

Governing equations and the boundary conditions are non-dimensionalized by introducing the following non-dimensional variables.

$$X = x/H,\ Y = y/H,\ U_f = u_f/u_{ref},\ U_i = u_i/u_{ref},\ U_p = u_p/u_{ref},\ P = p/\rho u_{ref}^2,\ \theta_f = (T_f - T_e)/(qH/k_f),\ \theta_p = (T_p - T_e)/(qH/k_f) \quad (1)$$

D Bhargavi and J. Sharath Kumar Reddy are with the Department of Mathematics, NIT Warangal, Telangana, India-506004 (e-mail: bhargavi@nitw.ac.in, jskreddy.amma@gmail.com).

In (1), X and Y are the non-dimensional coordinates. U and P are the non-dimensional velocity and pressure. The subscripts f and p refer to fluid and porous regions. θ {θ_f in the fluid region and θ_p in the porous region} is the non-dimensional temperature. u_{ref} is the average velocity through the channel. u_{ref} is related to u_p and u_f by,

$$\frac{2}{H}\left[\int_{-H/2}^{\frac{H}{2}+\frac{l_p}{2}} u_p dy + \int_{\frac{H}{2}+\frac{l_p}{2}}^{0} u_f dy\right] = u_{ref} \tag{2}$$

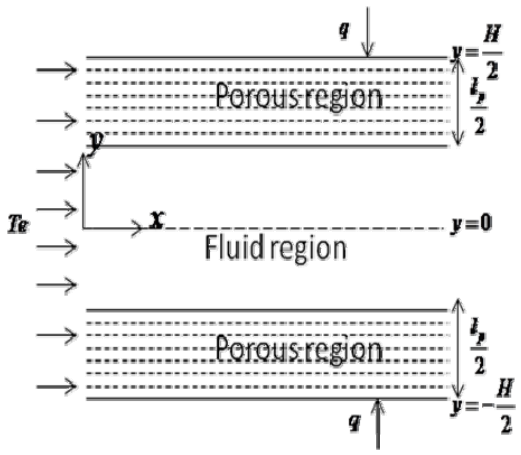

(a) Dimensional

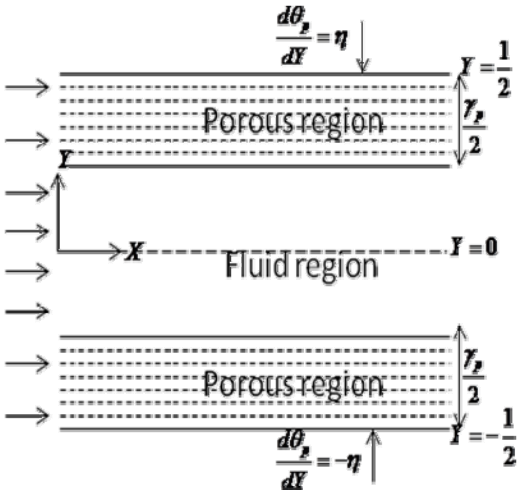

(b) Non Dimensional

Fig. 1 Physical Model and Coordinate System

On introducing the non-dimensional variables given in (1), the governing equations for conservation of momentum and energy applicable in the fluid and porous regions in non-dimensional form become:

A. Fluid Region

$$\frac{d^2U_f}{dY^2} = Re\ \frac{dP}{dX} \tag{3}$$

$$U_f\frac{\partial\theta_f}{\partial X^*} = A_c\frac{1}{Pe^2}\frac{\partial^2\theta_f}{\partial X^{*2}} + \frac{\partial^2\theta_f}{\partial Y^2} + Br\left(\frac{dU_f}{dY}\right)^2 \tag{4}$$

In (3), *Re*, the Reynolds number is defined by

$$Re = \rho u_{ref} H / \mu_f \tag{5}$$

In (4), *Pe*, Peclet number and *Br*, Brinkman number are defined by,

$$Pe = u_{ref} H / \alpha_f,\ Br = \mu_f {u_{ref}}^2 / qH \tag{6}$$

when $Br > 0$ represents, the fluid is getting cooled and $Br < 0$ represents the fluid is getting heated.

B. Porous Region

$$\frac{d^2U_p}{dY^2} - \frac{\varepsilon}{Da}U_p = \varepsilon\ Re\frac{dP}{dX} \tag{7}$$

$$U_p\frac{\partial\theta_p}{\partial X^*} = \frac{1}{\eta}\left(A_c\frac{1}{Pe^2}\frac{\partial^2\theta_p}{\partial X^{*2}} + \frac{\partial^2\theta_p}{\partial Y^2}\right) + \phi_i \tag{8}$$

In (8), ϕ_i is non-dimensional dissipation model is given by,

Darcy Model:

$$\phi_1 = \frac{Br}{Da}{U_p}^2 \tag{9}$$

Clear fluid compatible model:

$$\phi_2 = Br\left[\frac{{U_p}^2}{Da} + \left(\frac{dU_p}{dY}\right)^2\right] \tag{10}$$

In (7) *Da*, the Darcy number is defined by,

$$Da = K / H^2 \tag{11}$$

In (7) and (8), ε and η are defined by,

$$\varepsilon = \mu_f / \mu_{eff}\ ,\ \eta = k_f / k_{eff} \tag{12}$$

C. Non-Dimensional Boundary Conditions

The boundary and interfacial conditions take the following non-dimensional form

$$\frac{dU_f}{dY} = 0,\ \frac{\partial\theta_f}{\partial Y} = 0 \text{ at } Y = 0 \tag{13}$$

$$U_f = U_p = U_i,\ \frac{dU_f}{dY} = \frac{1}{\varepsilon}\frac{dU_p}{dY} \text{ at the interface } Y = -\frac{1}{2} + \frac{\gamma_p}{2} \quad (14)$$

$$\theta_f = \theta_p = \theta_i,\ \frac{\partial \theta_f}{\partial Y} = \frac{1}{\eta}\frac{\partial \theta_p}{\partial Y} \text{ at the interface } Y = -\frac{1}{2} + \frac{\gamma_p}{2} \quad (15)$$

$$U_p = 0,\ \frac{\partial \theta_p}{\partial Y} = -\eta \text{ at } Y = -1/2 \quad (16)$$

Inlet conditions

$$\theta_p(0, Y) = 0 \text{ for } -\frac{1}{2} \le Y \le -\frac{1}{2} + \frac{\gamma_p}{2} \quad (17)$$

$$\theta_f(0, Y) = 0 \text{ for } -\frac{1}{2} + \frac{\gamma_p}{2} \le Y \le 0 \quad (18)$$

$$\frac{\partial \theta_b}{\partial X^*} = 0 \Rightarrow \frac{\partial \theta_{f,p}}{\partial X^*} = \frac{\theta_{f,p}}{\theta^*}\frac{\partial \theta^*}{\partial X^*} \text{ at } X^* \ge X^*_{fd} \text{ for -1/2} \le Y \le 1/2$$
{downstream condition} (19)

In (19), θ_b is the non-dimensional temperature based on the bulk mean temperature defined by

$$\theta_b = \frac{T - T_e}{T_b - T_e} = \frac{\theta}{\theta^*} \quad (20)$$

III. Numerical Scheme: SAR

Numerical solutions to (4) and (8) along with the boundary conditions on θ given in (13)-(20) have been obtained employing the SAR scheme as described in [3], [15] and [16]. The fully developed velocity profiles in the fluid region, U_f and porous region, U_p have been taken from [16]. The application of numerical scheme, uniform, and non-uniform grid generation and numerical trials has been given in [16].

IV. Result and Discussion

It is assumed that $\varepsilon = \mu_f/\mu_{eff} = 1$ and $\eta = k_f/k_{eff} = 1$. The numerical solutions have been obtained for, $0.005 \le Da \le 0.01$, $\gamma_p = 0, 0.2, 0.4, 0.6, 0.8$ and 1.0, $-1.0 \le Br \le 1.0$ and $Pe = 5$, 25 and 100 and neglecting axial conduction (designated by $A_c = 0$) by the SAR scheme which has been extensively used for this class of problems [3], [15], [16]. The number of combinations of the parameters is very high; detailed computations have been performed and the results are available with the author. However, selected results needed to bring out the features arising out of including viscous dissipation have been presented here.

A. Channel Fully Filled with a Porous Medium

Thermal Field

Non-dimensional temperature in excess of wall temperature, $\theta_w - \theta_p$ profiles for $Da = 0.005$ and $\gamma_p = 1.0$ at different axial locations, X^* for (a) $Br = -0.5$ and (b) $Br = 0.5$ for the Darcy model are shown in Fig. 2 for $Pe = 5$ and Fig. 3 for $Pe = 100$ respectively. Similarly, non-dimensional temperature in excess of wall temperature, $\theta_w - \theta_p$ profiles for $Da = 0.005$ and $\gamma_p = 1.0$ at different X^* for (a) $Br = -0.5$ and (b) $Br = 0.5$ for the clear fluid compatible model are shown in Fig. 4 for $Pe = 5$ and Fig. 5 for $Pe = 100$ respectively.

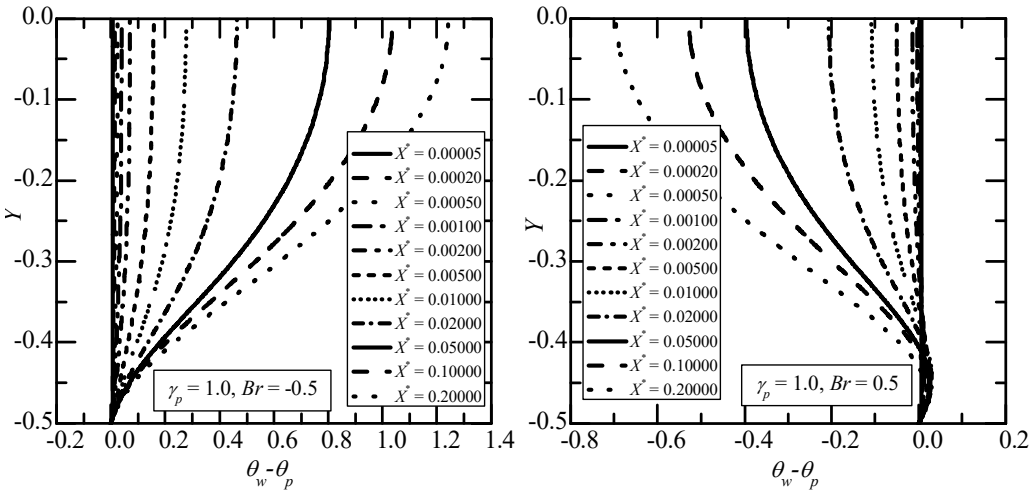

(a) (b)

Fig. 2 Variation of non-dimensional temperature excess of wall temperature $\theta_w - \theta_p$ profiles for Da = 0.005 and $\gamma_p = 1.0$ for $Pe = 5$ at different X^* for (a) $Br = -0.5$ and (b) $Br = 0.5$ for Darcy model

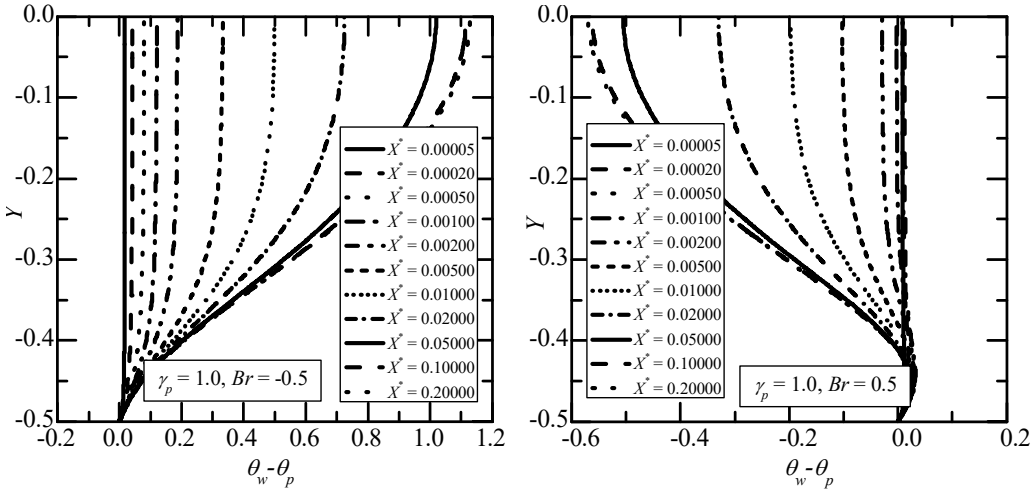

(a) (b)

Fig. 3 Variation of non-dimensional temperature excess of wall temperature $\theta_w - \theta_p$ profiles for Da = 0.005 and $\gamma_p = 1.0$ for Pe = 100 at different X^* for (a) $Br = -0.5$ and (b) $Br = 0.5$ for Darcy model

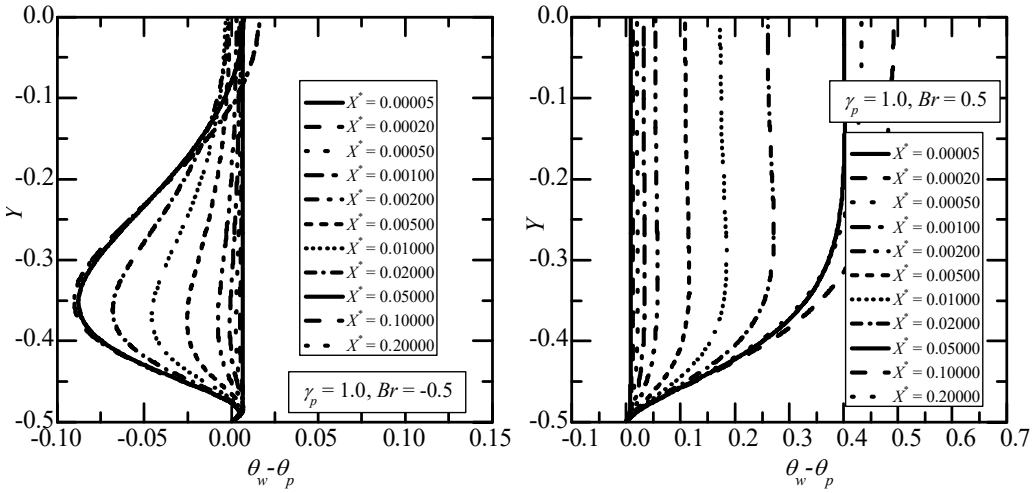

(a) (b)

Fig. 4 Variation of non-dimensional temperature excess of wall temperature $\theta_w - \theta_p$ profiles for Da = 0.005 and $\gamma_p = 1.0$ for Pe = 5 at different X^* for (a) $Br = -0.5$ and (b) $Br = 0.5$ for the clear fluid compatible model

The non-dimensional temperature in excess of wall temperature, $\theta_w - \theta_p$ profiles for γ_p = 1.0 obtained using Darcy model [17] given in Figs. 2 and 3 {(9) applied for − 0.5 ≤ Y ≤ 0 because of symmetry of the channel} are not similar to those shown in Figs. 4 and 5 for a clear fluid compatible model [18] (10).

The difference in the $\theta_w - \theta_p$ profiles for the two dissipation models can be found even when Da is high. The difference in the profiles shown in Figs. 2, 3 and Figs. 4, 5 emerge from the dissipation function employed, for the Darcy model and the clear fluid compatible model. It is clear that Pe = 5 (lowest of the values computed) represents the strongest axial conduction effect while Pe = 100 shows an almost negligible axial conduction effect.

On examining Figs. 2 and 3 for the Darcy model and Figs. 4 and 5 for clear fluid compatible model, the following conclusions emerge by comparing $\left(\theta_w - \theta_p\right)_{Br\neq 0}$ with

$$\left(\theta_w - \theta_p\right)_{Br=0}, \left(\theta_w - \theta_p\right)_{Br<0} > \left(\theta_w - \theta_p\right)_{Br=0} \text{ and}$$
$$\left(\theta_w - \theta_p\right)_{Br>0} < \left(\theta_w - \theta_p\right)_{Br=0} \quad (21)$$

The relation given in (21) is satisfied for Darcy model.

$$\left(\theta_w - \theta_p\right)_{Br<0} < \left(\theta_w - \theta_p\right)_{Br=0} \text{ and}$$
$$\left(\theta_w - \theta_p\right)_{Br>0} > \left(\theta_w - \theta_p\right)_{Br=0} \quad (22)$$

The relation given in (22) is satisfied for the clear fluid compatible model.

In the thermally developing region, the values of the temperature difference, $\left(\theta_w - \theta_p\right)_{Br\neq 0}$ and the limiting values of $\left(\theta_w - \theta_{p,CL}\right)_{Br\neq 0}$ given in [19], depend on the Brinkman number for both dissipation models. As per our definition, $Br > 0$ represents fluid getting cooled and dissipation prevents the fluid from cooling down to wall temperature, leaving $\left(\theta_w - \theta_p\right)_{Br>0} < 0$. Similarly when $Br < 0$, the fluid is getting heated and the fluid exceeds the wall temperature making $\left(\theta_w - \theta_p\right)_{Br<0} > 0$ for the Darcy model whereas, in the case of the clear fluid compatible dissipation model, $\left(\theta_w - \theta_p\right)_{Br>0} > 0$ for $Br > 0$ and $\left(\theta_w - \theta_p\right)_{Br<0} < 0$ for $Br < 0$.

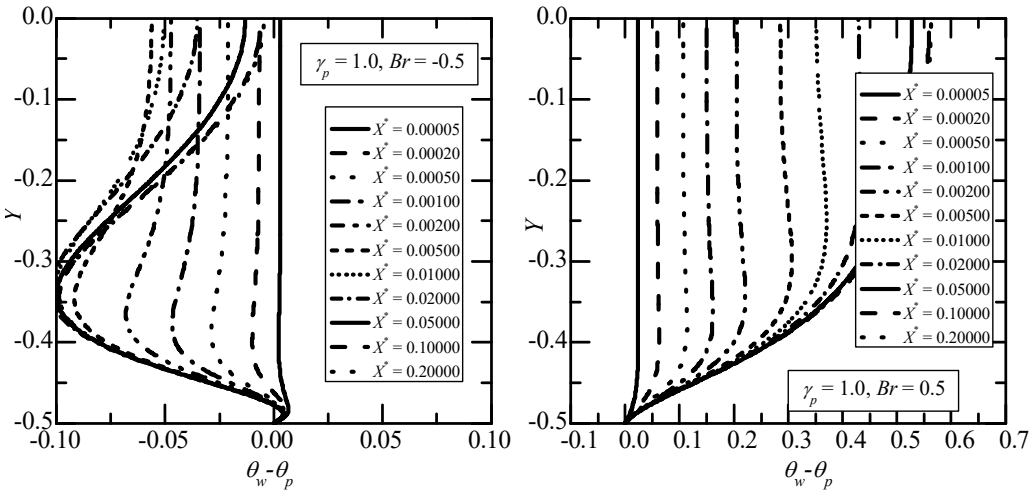

(a) (b)

Fig. 5 Variation of non-dimensional temperature excess of wall temperature $\theta_w - \theta_p$ profiles for Da = 0.005 and $\gamma_p = 1.0$ for Pe = 100 at different X^* for (a) $Br = -0.5$ and (b) $Br = 0.5$ for the clear fluid compatible model

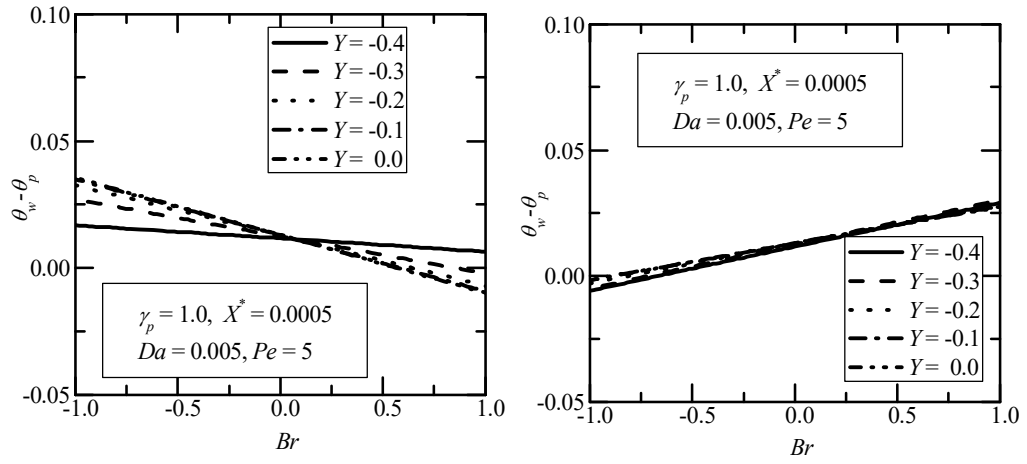

(a) Darcy model (b) Clear fluid compatible model

Fig. 6 Variation of non-dimensional temperature excess of wall temperature $\theta_w - \theta_p$ profiles vs. Br for Da = 0.005 and $\gamma_p = 1.0$ for Pe = 5 at X^* = 0.0005 for (a) the Darcy model and (b) the clear fluid compatible model

Plots of $\theta_w - \theta_p$ vs. Br are shown in Fig. 6 for (a) Darcy model (b) clear fluid compatible model for Pe = 5, when axial conduction has been included at X^* = 0.0005 for different Y = -0.4, -0.3, -0.2, -0.1 and 0.0 for Da = 0.005 for γ_p =1.0. From Fig. 6, $\theta_w - \theta_p$ does vary linearly with Br for both models. This fact is also true when axial conduction is neglected.

Local Nusselt Number

Variation of local Nusselt number with X^* for (a) $Br \leq 0$ and (b) $Br \geq 0$ for the Darcy model and the clear fluid compatible model are shown in Figs. 7 and 8 respectively for Da = 0.005 when the axial conduction is neglected (A_c = 0).

From Figs. 7 and 8, it is apparent that Nu_{px} displays an

unbounded swing for $Br > 0$ at, say, X^*_{sw} for the Darcy model. On the other hand for the clear fluid compatible model, Nu_{px} displays an unbounded swing for $Br < 0$ at X^*_{sw}. Nu_{px}, displays an unbounded swing since the bulk mean temperature reaches the wall temperature and exceeds it because of viscous dissipation. This fact is the same in the case of the clear fluid channels ($\gamma_p = 0$). This fact is reported for $\gamma_p = 0$ when channel walls are subjected to constant temperature [4], [20]. Also, Nu_{px}, increases as Br increases for the Darcy model when $Br \leq 0$ whereas, Nu_{px}, decreases as Br increases for the clear fluid compatible model when $Br \geq 0$.

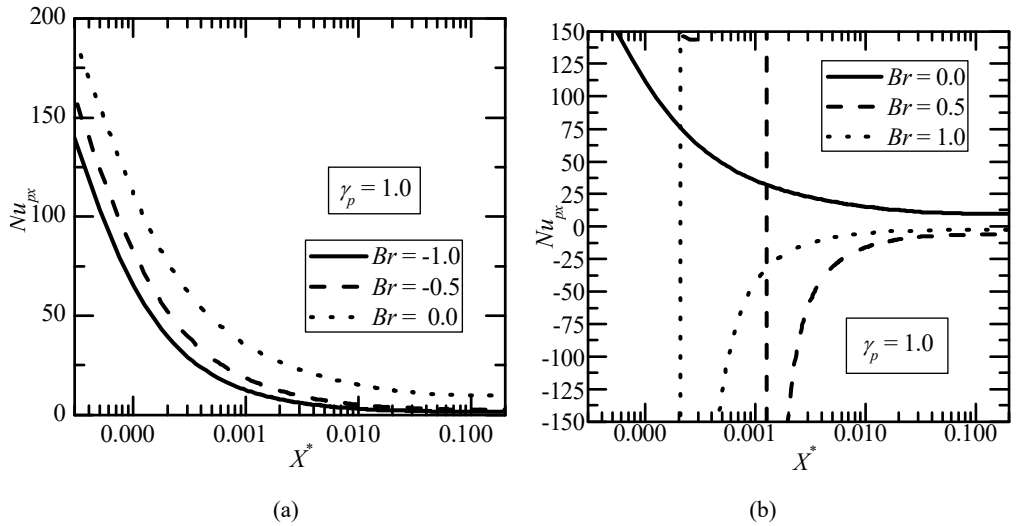

(a) (b)

Fig. 7 Variation of local Nusselt number with X^* for $\gamma_p = 1.0$ and Da = 0.005 for (a) $Br \leq 0$ (b) $Br \geq 0$ for Darcy model when axial conduction neglected (A_c = 0)

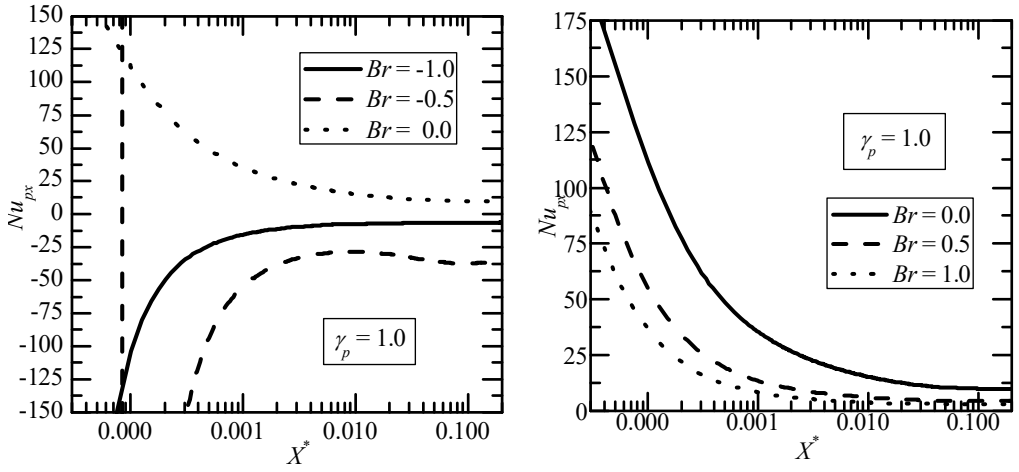

(a) (b)

Fig. 8 Variation of local Nusselt number with X^* for $\gamma_p = 1.0$ and Da = 0.005 for (a) $Br \leq 0$ (b) $Br \geq 0$ for clear fluid compatible model when axial conduction neglected (A_c = 0)

Variation of local Nusselt number with X^* for Da = 0.005 and $\gamma_p = 1.0$ for different Peclet numbers, Pe = 5, 25 and 100 for (a) $Br = -0.5$ and (b) $Br = 0.5$, are shown in Figs. 9 and 10 for the Darcy model and the clear fluid compatible model respectively.

From Figs. 9 and 10, Nu_{px} displays an unbounded swing, X^*_{sw} for $Br > 0$ for Darcy model whereas, for the clear fluid compatible model, Nu_{px} displays an unbounded swing, X^*_{sw} for $Br < 0$. For both models, at low Peclet number, the value of the X^*_{sw} is high. Also Nu_{px}, decreases as Pe increases for Darcy model when $Br < 0$. But for the clear fluid compatible model, Nu_{px}, decreases as Pe increases when $Br > 0$. This model is consistent with the clear fluid channel in the behavior of Nusselt number with X^* for all Da and Pe.

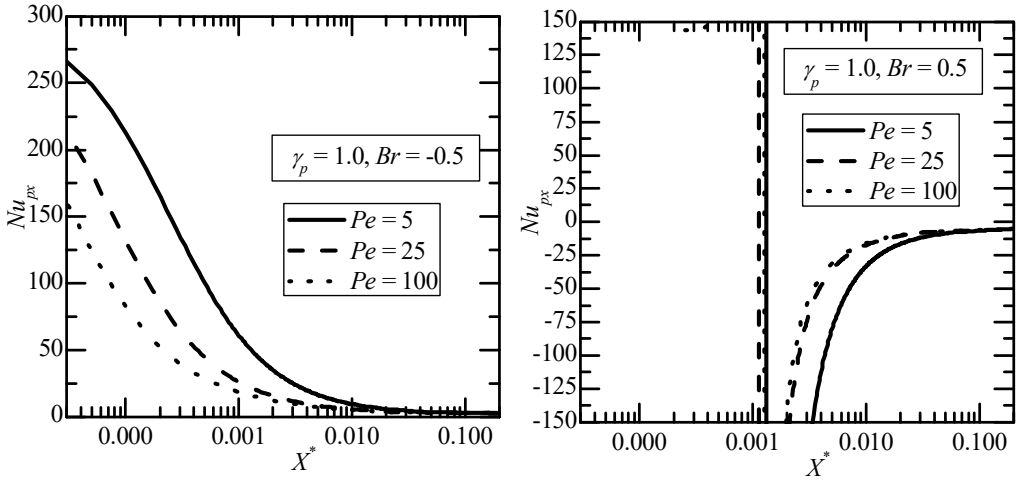

(a) (b)

Fig. 9 Variation of local Nusselt number with X^* for Da = 0.005 for different Peclet numbers, Pe at (a) $Br = -0.5$ (b) $Br = 0.5$ for Darcy model

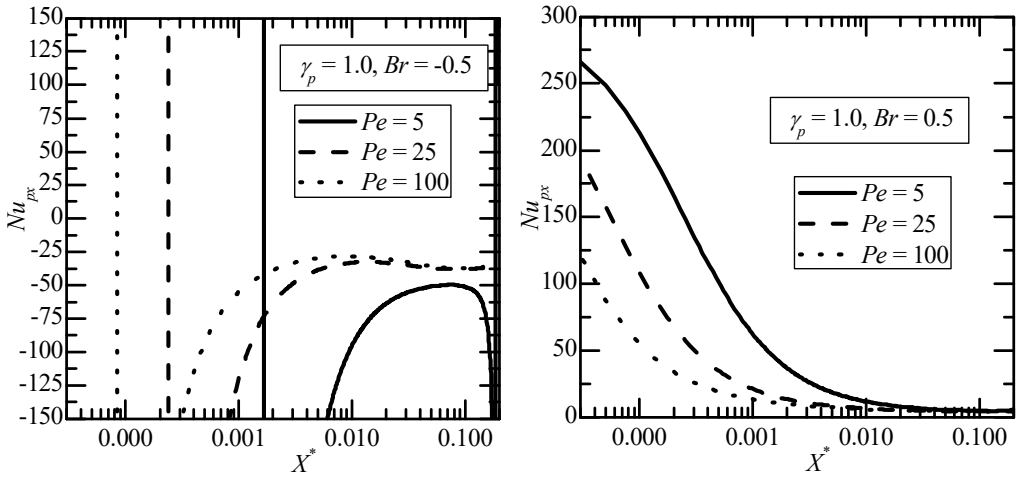

(a) (b)

Fig. 10 Variation of local Nusselt number with X^* for Da = 0.005 for different Peclet numbers, Pe at (a) $Br = -0.5$ (b) $Br = 0.5$ for the clear fluid compatible model

B. Channel Partially Filled with a Porous Medium

Thermal Field

Non-dimensional temperature excess of wall temperature profiles, $\theta_w - \theta_p, \theta_w - \theta_f$ for Da = 0.005, Pe = 5 and $Br = -0.5,\ 0,\ 0.5$ at X^* = 0.005 for (a) $\gamma_p = 0.2$ and (b) $\gamma_p = 0.8$ are shown in Figs. 11 and 12 for the Darcy and the clear fluid compatible model respectively.

On examining Figs. 11 (a) and (b) for the Darcy model and Figs. 12 (a) and (b) for the clear fluid compatible model, the following conclusions emerge by comparing $\left(\theta_w - \theta_{f,p}\right)_{Br\neq 0}$ with $\left(\theta_w - \theta_{f,p}\right)_{Br=0}$,

$$\left(\theta_w - \theta_{f,p}\right)_{Br<0} < \left(\theta_w - \theta_{f,p}\right)_{Br=0} \text{ and}$$

$$\left(\theta_w - \theta_{f,p}\right)_{Br>0} > \left(\theta_w - \theta_{f,p}\right)_{Br=0} \tag{23}$$

$$\left(\theta_w - \theta_{f,p}\right)_{Br<0} > \left(\theta_w - \theta_{f,p}\right)_{Br=0} \text{ and}$$
$$\left(\theta_w - \theta_{f,p}\right)_{Br>0} < \left(\theta_w - \theta_{f,p}\right)_{Br=0} \tag{24}$$

The relations are given in (23) and (24) are valid for all porous fraction in the fluid region and porous regions respectively for both models.

Plots of $\theta_w - \theta_{f,p}$ vs. Br are shown in Fig. 13 for the Darcy model and Fig. 14 for the clear fluid compatible model for Pe = 5, when axial conduction has been included at X^* = 0.0005 for different Y = -0.4, -0.3, -0.2, -0.1 and 0.0 for Da = 0.005 for (a) γ_p = 0.2 and (b) γ_p = 0.8. From Figs. 13 and 14, $\theta_w - \theta_p$ does vary linearly with Br for both models. This fact is true

even when axial conduction is neglected.

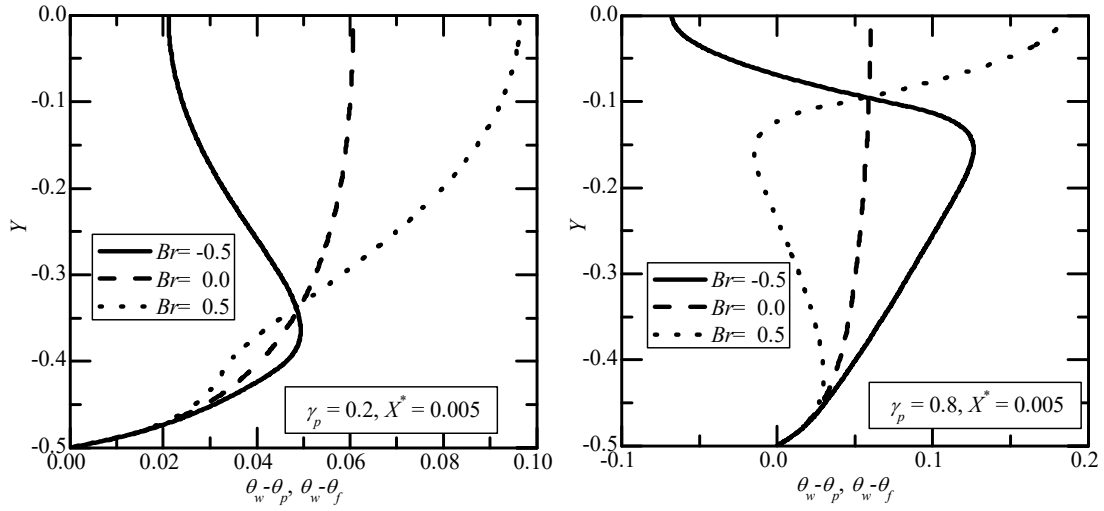

Fig. 11 Variation of non-dimensional temperature excess of wall temperature $\theta_w-\theta_p, \theta_w-\theta_f$ profiles for *Da* = 0.005, *Pe* = 5 and $Br = -0.5,\ 0,\ 0.5$ at X^* = 0.005 for (a) $\gamma_p = 0.2$ and (b) $\gamma_p = 0.8$ for Darcy model

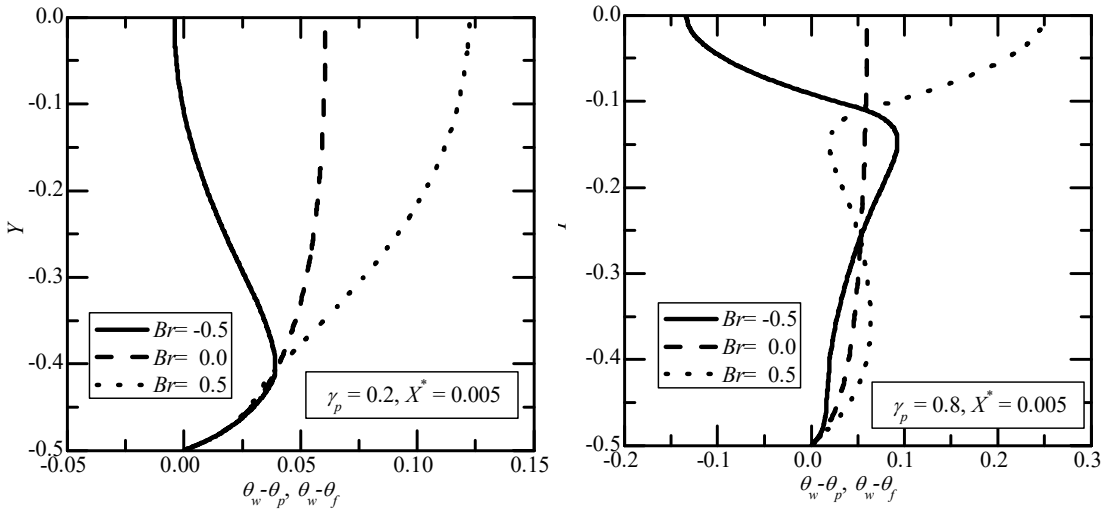

Fig. 12 Variation of non-dimensional temperature excess of wall temperature $\theta_w-\theta_p, \theta_w-\theta_f$ profiles for *Da* = 0.005, *Pe* = 5 and $Br = -0.5,\ 0,\ 0.5$ at X^* = 0.005 for (a) $\gamma_p = 0.2$ and (b) $\gamma_p = 0.8$ for the clear fluid compatible model

Local Nusselt Numbers

Variation of local Nusselt number with X^* for *Da* = 0.005, $\gamma_p = 0.2$ and *Pe* = 5 for (a) $Br \le 0$ and (b) $Br \ge 0$ is shown in Figs. 15 and 16 for Darcy and clear fluid compatible models respectively. Similarly, variation of local Nusselt number with X^* for *Da* = 0.005, $\gamma_p = 0.8$ and *Pe* = 5 for (a) $Br \le 0$ and (b) $Br \ge 0$ is shown in Figs. 17 and 18 for Darcy and clear fluid compatible models respectively.

From Figs. 15-18, for both models, Nu_{px} reveals an unbounded swing for *Br* < 0 at axial value X^*_{sw}. This unbounded swing X^*_{sw} happens for the porous fraction, $\gamma_p \le 0.8$. Also, for both models, Nu_{px} decreases as *Br* increases when *Br* > 0 for the porous fractions with $\gamma_p \le 0.8$. As porous fraction increases, X^*_{sw} increases for the Darcy model whereas X^*_{sw} decreases as porous fraction increases in the clear fluid compatible dissipation model.

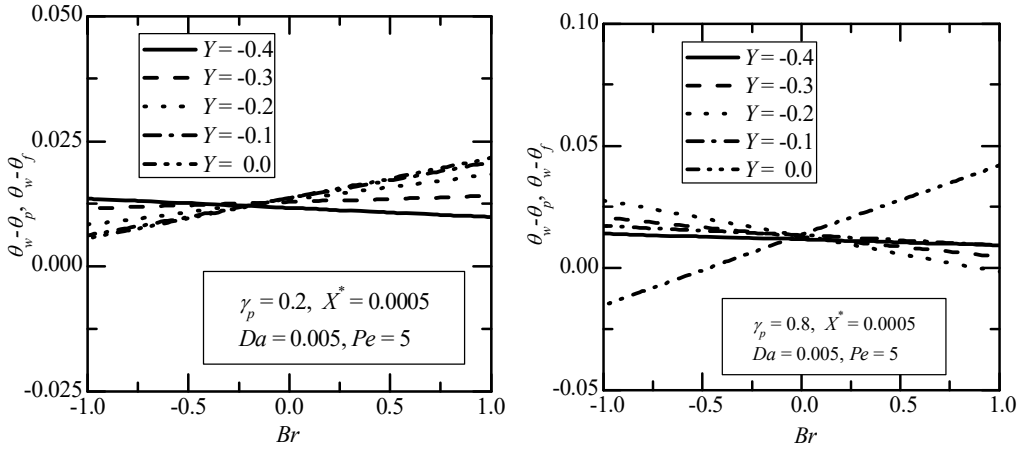

Fig. 13 Variation of non-dimensional temperature excess of wall temperature $\theta_w - \theta_p, \theta_w - \theta_f$ profiles vs. *Br* for *Da* = 0.005 for *Pe* = 5 at X^* = 0.0005 for (a) $\gamma_p = 0.2$ and (b) $\gamma_p = 0.8$ for the Darcy model

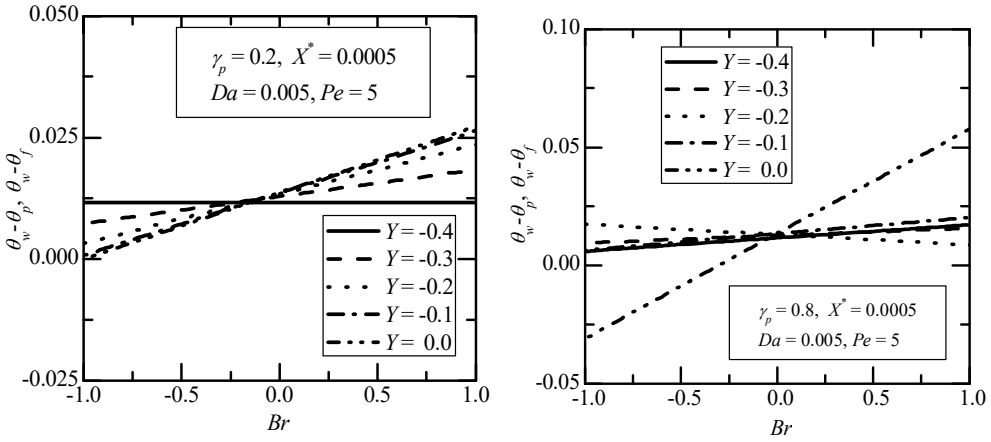

Fig. 14 Variation of non-dimensional temperature excess of wall temperature $\theta_w - \theta_p, \theta_w - \theta_f$ profiles vs. *Br* for *Da* = 0.005 for *Pe* = 5 at X^* = 0.0005 for (a) $\gamma_p = 0.2$ and (b) $\gamma_p = 0.8$ for the clear fluid compatible model

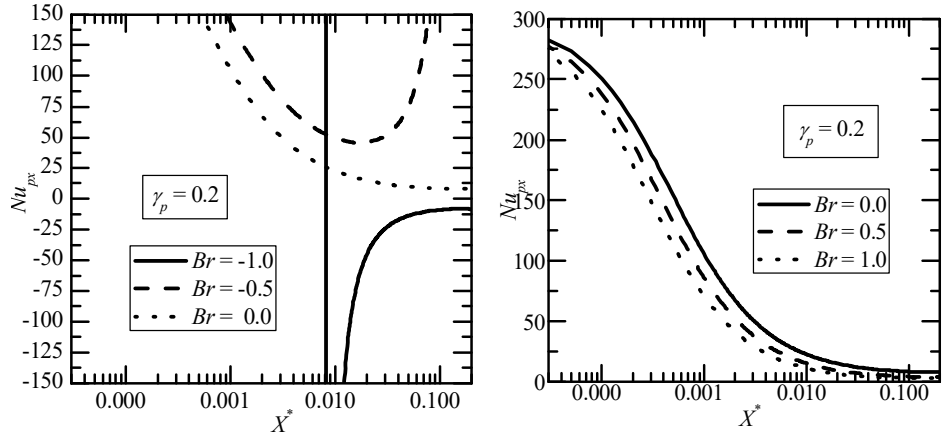

Fig. 15 Variation of the local Nusselt number with X^* for *Da* = 0.005, $\gamma_p = 0.2$ and *Pe* = 5 for (a) $Br \le 0$ and (b) $Br \ge 0$ for Darcy model

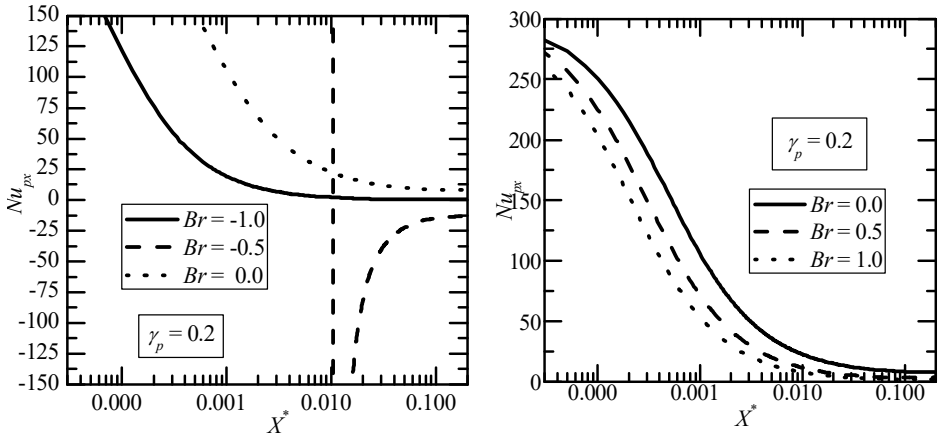

Fig. 16 Variation of the local Nusselt number with X^* for $Da = 0.005$, $\gamma_p = 0.2$ and $Pe = 5$ for (a) $Br \le 0$ and (b) $Br \ge 0$ for clear fluid compatible model

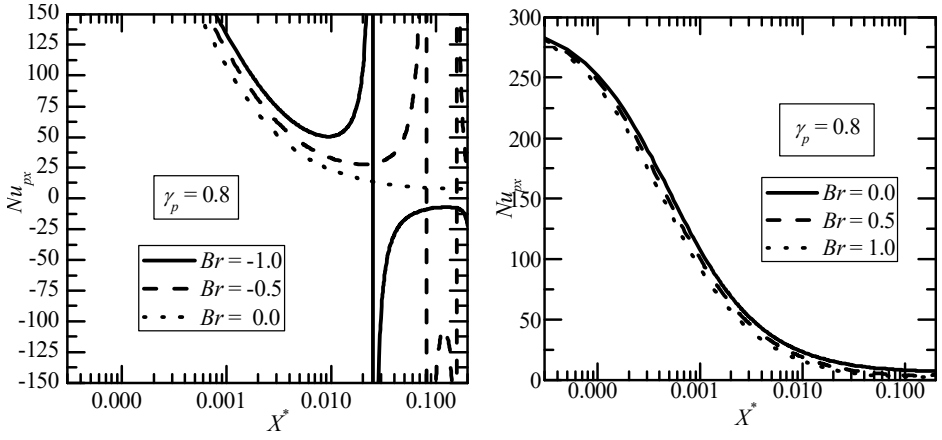

Fig. 17 Variation of local Nusselt number with X^* for $Da = 0.005$, $\gamma_p = 0.8$ and $Pe = 5$ for (a) $Br \le 0$ and (b) $Br \ge 0$ for Darcy model

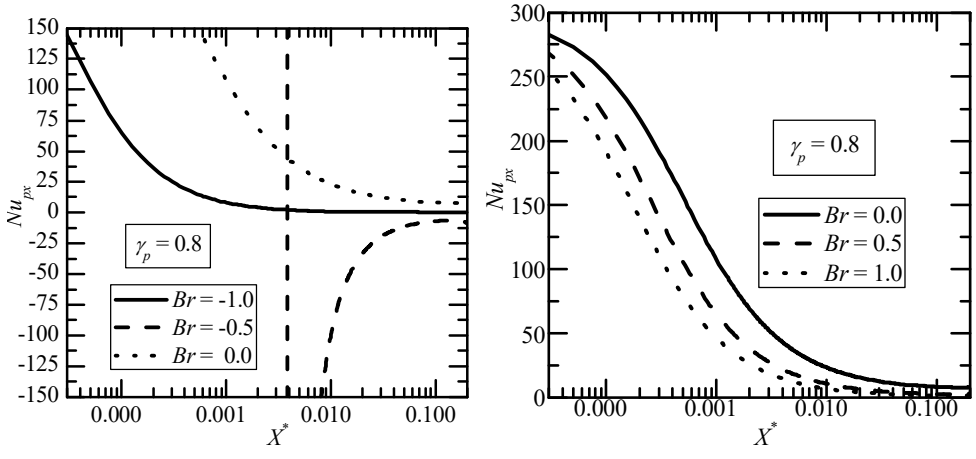

Fig. 18 Variation of local Nusselt number with X^* for $Da = 0.005$, $\gamma_p = 0.8$ and $Pe = 5$ for (a) $Br \le 0$ and (b) $Br \ge 0$ for Clear fluid compatible model

Nusselt Number Changes with a Porous Fraction

To examine the changes of the local Nusselt number with a porous fraction, plots are given at the entry locations of the channel. Variation of the local Nusselt number, Nu_{px} with γ_p, for different Darcy numbers, Da = 0.005, 0.01 for Pe = 5 for $Br = 0.5$ at (a) X^*= 0.0005 and at (b) X^*= 0.005 is shown in Fig. 19 for Darcy model. From Fig. 19, it is clear that there is no maximum or minimum in local Nusselt number at a given porous fraction other than γ_p = 0 and 1.0. Hence we cannot have enhancement or reduction in the local Nusselt number at a given porous fraction in the case of Darcy model.

Variation of the local Nusselt number, Nu_{px} with γ_p, for different Darcy numbers, Da = 0.005, 0.01 for Pe = 5 for $Br = 0.5$ at (a) X^*= 0.0005 and at (b) X^*= 0.005 is shown in Fig. 20 for the clear fluid compatible model. It can be seen from Figs. 20 (a) and (b) that the maximum value in local Nusselt number occurs at $\gamma_p \approx 0.2$ while the minimum occurs in Nu_{px} for $\gamma_p \approx 0.6$. The minimum and maximum values do not depend on the axial location of X^*.

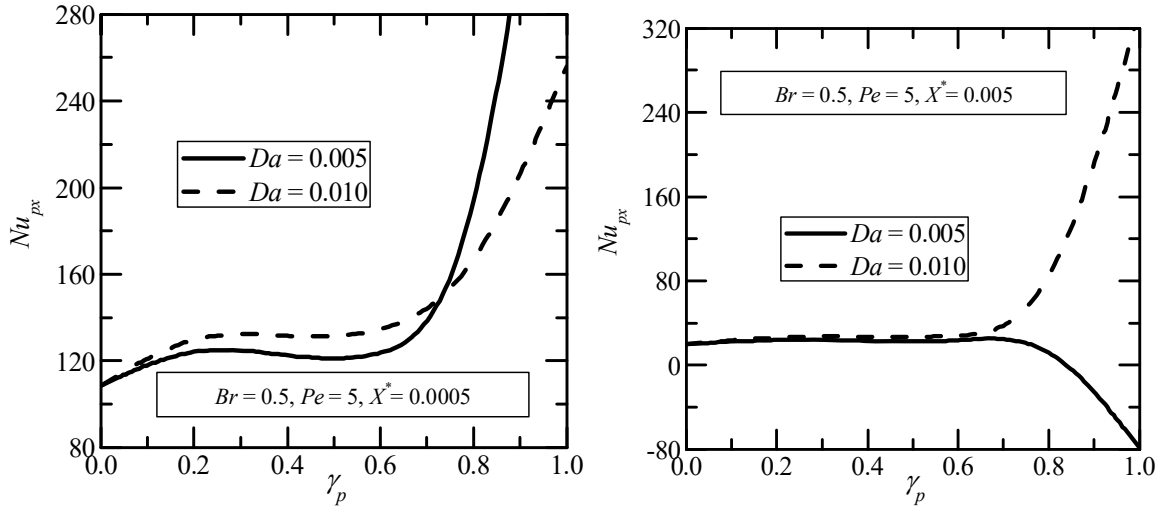

(a) X^*= 0.0005 (b) X^*= 0.005

Fig. 19 Variation of local Nusselt number with γ_p, for different Darcy numbers, Da = 0.005, 0.01 and Pe = 5 at (a) X^*= 0.0005 and (b) X^*= 0.005 for $Br = 0.5$ for the Darcy model

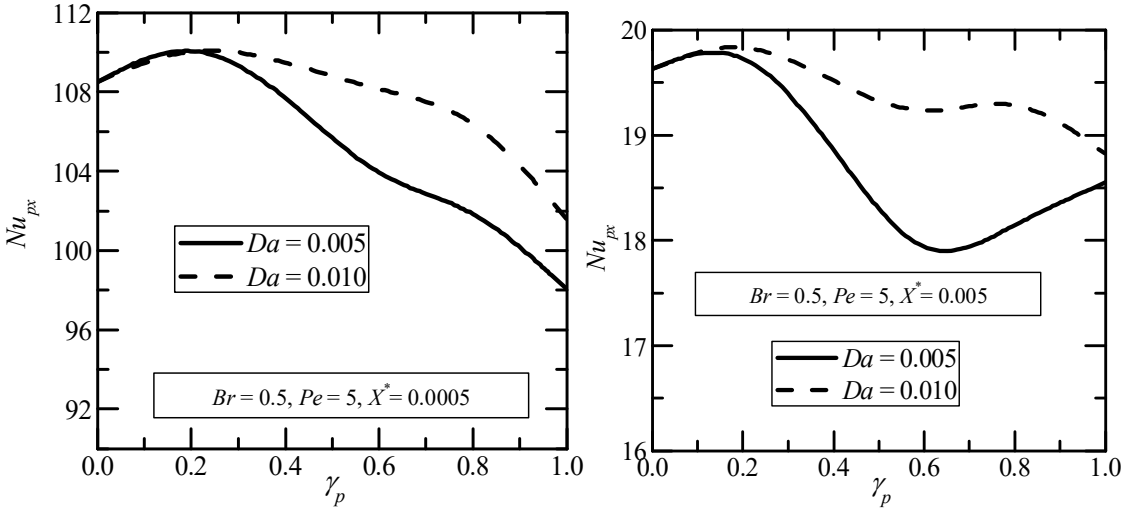

(a) X^*= 0.0005 (b) X^*= 0.005

Fig. 20 Variation of local Nusselt number with γ_p, for different Darcy numbers, Da = 0.005, 0.01 and Pe = 5 at (a) X^*= 0.0005 and (b) X^*= 0.005 for $Br = 0.5$ for the clear fluid compatible model

V. Conclusions

Two dissipation models, namely, a) Darcy model due to [17] and b) the clear fluid compatible model due to [18] have been employed in the porous region. The conventional dissipation function {see [21]} has been employed in the fluid region. Brinkman number, *Br*, characterizes the viscous dissipation. As defined in the present paper, $Br > 0$ represents fluid getting cooled while $Br < 0$ indicates the fluid getting heated.

Nusselt number displays an unbounded swing at some $X^* = X^*_{sw}$ when $Br < 0$. X^*_{sw} decreases as *Br* decreases, i.e., for larger negative values of *Br*. The limiting values of the Nusselt numbers (for large X^*) on the fluid and porous sides, Nu_{px} are dependent on *Br* for all $Br \neq 0$ in the developing region also. These limiting values depend on the porous fraction too. Nu_{px}, decreases as X^* increases for all porous fractions when $Br > 0$. Nu_{px}, decreases as *Br* increases for all porous fractions when $Br > 0$. These results are true for both models when the channel is partially filled with porous material. When fully filled with porous material channels, Nu_{px} increases as *Br* increases for $Br < 0$ in Darcy model. On the contrary, in the case of the clear fluid compatible model, Nu_{px}, decreases as *Br* increases for $Br > 0$. The qualitative behavior of Nu_{px}, in the channels partially filled with porous material ($0 < \gamma_p < 1.0$) and the channel fully filled with porous material ($\gamma_p = 1.0$) for the clear fluid compatible model given in (10) is the same as that of clear fluid channel ($\gamma_p = 0$). This fact is reported in [4] and [20] for ducts subjected to the constant wall temperature. However, this qualitative behavior of Nu_{px} is not the same in the Darcy model when compared with clear fluid channel. Hence clear fluid compatible dissipation model is more suitable for porous region than Darcy model

References

[1] Agrawal, H. C., Heat Transfer in Laminar Flow between Parallel Plates at Small Peclet Numbers, Appl. Sci. Res., vol 9, pp. 177-189, 1960.
[2] Hennecke, D. K., Heat Transfer by Hagen-Poiseuille Flow in the Thermal Development Region with Axial Conduction, Warme- und Stoffubertragung., vol 1, pp. 177-184, 1968.
[3] Ramjee Repaka and Satyamurty, V. V., Local and Average Heat Transfer in the Thermally Developing Region of an Asymmetrically Heated Channel, Int. J. Heat Mass Transfer, 53, pp. 1654-1665, 2010.
[4] Mohan Jagadeesh Kumar, M., Effect of Axial Conduction and Viscous Dissipation on Heat Transfer for Laminar Flow through a Circular Pipe, Perspectives in Science, vol 8, pp. 61-65, 2016.
[5] Lundberg, R. E., Mccuen, P. A. and Reynolds, W.C., Heat Transfer in Annular Passages. Hydro dynamically Developed Laminar Flow with Arbitrarily Prescribed Wall Temperatures or Heat Fluxes, Int. J. Heat Mass Trans., vol 6, pp. 495-529, 1963.
[6] Worsoe-Schmidt, P. M., Heat Transfer in the Thermal Entrance Region Of Circular Tubes and Annular Passages with Fully Developed Laminar Flow, Int. J. Heat Mass Trans., vol 10, pp. 541-551, 1967.
[7] Nguyen, T. V. and Maclaine-cross, I. L., Simultaneously Developing, Laminar Flow, Forced Convection in the Entrance Region of Parallel Plates, J. heat trans., vol 113, pp. 837-842, 1991.
[8] Campo, A. and Salazar, A., Forced Convection-Axial Conduction Between Parallel Walls with Unequal Heat Fluxes, Warme- und Stoffubertragung., vol 20, pp. 177-181, 1986.
[9] Xiong, M., Thermally Developing Forced Convection in a Porous Medium: Parallel-Plate Channel or Circular Tube with Walls at Constant Heat Flux, J. Porous Media., vol 6, 2003.
[10] Shah, R. K. and London, A. L., Laminar Flow Forced Convection in Ducts, Advances in Heat Transfer. Supplement 1, Academic Press, New York, 1978.
[11] Nguyen, T. V., Laminar heat transfer for thermally developing flow in ducts, Int. J. Heat Mass Trans., vol 35, pp. 1733-1741, 1992.
[12] Hooman, K., Haji-sheik, A. and Nield, D.A., Thermally developing Brinkman–Brinkman forced convection in rectangular ducts with isothermal walls, Int. J. Heat and Mass Trans., vol 50, pp. 3521–3533, 2007.
[13] Kuznetsov, A. V., Xiong, M. and Nield, D. A., Thermally Developing Forced Convection in a Porous Medium: Circular Duct with Walls at Constant Temperature, with Longitudinal Conduction and Viscous Dissipation Effects, Transport in Porous Media, vol 53, pp. 331–345, 2003.
[14] Nield, D. A., Kuznetsov, A. V. and Xiong, M., Thermally Developing Forced Convection in a Porous Medium: Parallel Plate Channel with Walls at Uniform Temperature, with Axial Conduction and Viscous Dissipation Effects, Int. J. Heat and Mass Trans., vol 46, pp. 643-651, 2003.
[15] Satyamurty, V. V. and Bhargavi, D., Forced Convection in Thermally Developing Region of a Channel Partially Filled with a Porous Material and Optimal Porous Fraction, Int. J. Thermal Sciences, vol 49, pp. 319-332, 2010.
[16] Bhargavi, D. and Sharath Kumar Reddy, J., Effect of Heat Transfer in the Thermally Developing Region of the Channel Partially Filled with a Porous Medium: Constant Wall Heat Flux, Int. J. Thermal Sci., vol 130, pp. 484-495, 2018.
[17] Bejan, A., Convection Heat Transfer. Wiley, New York, 1984.
[18] Al-Hadhrami, A.K., Elliott, L. and Ingham, D.B., A New Model for Viscous Dissipation In Porous Media Across a Range of Permeability Values, Trans. Porous Media, vol. 53, pp. 117-122, 2003.
[19] Bhargavi, D. and Sharath Kumar Reddy, J., Analytical Investigation of Laminar Forced Convection with Viscous Dissipation in Parallel Plate Channels Partially Filled with a Porous Material: Constant Wall Heat Flux, Journal of Nanofluids, Volume 8, pp. 1-14, 2019.
[20] Ramjee, R. and Satyamurty, V. V., Effect of Viscous Dissipation on Forced Convection Heat Transfer in Parallel Plate Channels with Asymmetric Boundary Conditions", Proceedings of the ASME, International Mechanical Engineering Congress and Exposition IMECE2013 November 15-21, 2013, San Diego, California, USA.
[21] Schlichting, H. and Gersten, K., Boundary Layer Theory, Springer-Verlag, 2007.